NASA TECHNICAL NOTE

NASA TN D-6010

NASA TN D-6010

DOSE RESPONSE FUNCTIONS IN THE ATMOSPHERE DUE TO INCIDENT HIGH-ENERGY PROTONS WITH APPLICATION TO SOLAR PROTON EVENTS

by John W. Wilson, Jules J. Lambiotte, Jr., Trutz Foelsche, and Tassos A. Filippas

Langley Research Center
Hampton, Va. 23365

NATIONAL AERONAUTICS AND SPACE ADMINISTRATION • WASHINGTON, D. C. • NOVEMBER 1970

1. Report No.	2. Government Accession No.	3. Recipient's Catalog No.
NASA TN D-6010		

4. Title and Subtitle	5. Report Date
DOSE RESPONSE FUNCTIONS IN THE ATMOSPHERE DUE TO INCIDENT HIGH-ENERGY PROTONS WITH APPLICATION TO SOLAR PROTON EVENTS	November 1970
	6. Performing Organization Code
7. Author(s) John W. Wilson, Jules J. Lambiotte, Jr., Trutz Foelsche, and Tassos A. Filippas	8. Performing Organization Report No. L-6947
	10. Work Unit No. 720-04-10-02
9. Performing Organization Name and Address NASA Langley Research Center Hampton, Va. 23365	11. Contract or Grant No.
	13. Type of Report and Period Covered Technical Note
12. Sponsoring Agency Name and Address National Aeronautics and Space Administration Washington, D.C. 20546	14. Sponsoring Agency Code

15. Supplementary Notes

16. Abstract

The results of a recent high-energy nucleon transport calculation are presented as dose response functions at five altitudes in the atmosphere. The dose in extremities and the dose averaged over the body are directly calculated from these response functions by integration over the incident-energy spectra in the range 0.1 to 10 GeV. A dose-altitude profile is obtained by using all five sets of response functions. Also presented is a geomagnetic cutoff model for normal magnetic field strengths. Doses for several solar events of solar cycle 19, including the high-energy event of February 23, 1956, are presented. The present results are compared with other calculations.

17. Key Words (Suggested by Author(s))	18. Distribution Statement
Radiation dosage Secondary cosmic rays Protons Neutrons Gamma rays	Unclassified – Unlimited

19. Security Classif. (of this report)	20. Security Classif. (of this page)	21. No. of Pages	22. Price*
Unclassified	Unclassified	31	$3.00

*For sale by the Clearinghouse for Federal Scientific and Technical Information
Springfield, Virginia 22151

DOSE RESPONSE FUNCTIONS IN THE ATMOSPHERE DUE TO INCIDENT HIGH-ENERGY PROTONS WITH APPLICATION TO SOLAR PROTON EVENTS

By John W. Wilson, Jules J. Lambiotte, Jr.,
Trutz Foelsche, and Tassos A. Filippas
Langley Research Center

SUMMARY

The results of a recent high-energy nucleon-transport calculation are presented as dose response functions at five altitudes in the atmosphere. The dose in extremities and the dose averaged over the body are directly calculated from these response functions by integration over the incident-energy spectra in the range 0.1 to 10 GeV. A dose-altitude profile is obtained by using all five sets of response functions. Also presented is a geomagnetic-cutoff model for normal magnetic-field strengths. Doses for several solar events of solar cycle 19, including the high-energy event of February 23, 1956, are presented. The present results are compared with other calculations.

INTRODUCTION

Flamm and Lingenfelter (ref. 1) calculated the dose in the atmosphere for idealized solar proton spectra. They used rigidity spectra of the form $N = N_0 \exp(-P/P_0)$, where P is particle rigidity, N is the number of protons with rigidity greater than P, and N_0 and P_0 are parameters. (The parameter P_0 assumed values in the range 75 MV/c to 350 MV/c.) The experimental total nonelastic cross section and multiplicity were used. It was assumed in their calculations that the incident energy was equally shared among all secondary particles. Their results are of limited usefulness since many important solar spectra cannot be well represented by an exponential rigidity spectrum (ref. 2). Furthermore, the energy ranges of the most important solar events are not covered by these calculations.

Leimdorfer et al. (ref. 3) used a rigidity spectrum with $P_0 = 100$ MV/c and a Monte Carlo transport code to calculate dose in the atmosphere. They used the model of Bertini (ref. 4), which is an intranuclear cascade followed by evaporation, to calculate nuclear interactions. Leimdorfer et al. divided the incident-energy spectra from 50 to 450 MeV into 50 MeV groups and tabulated the dose due to each group. Their tabulations

are somewhat flexible because a variety of incoming spectra can be treated, but these spectra were cut off at an incoming energy of 450 MeV ($P < 1000$ MV/c). They considered the effects of shielding by an additional layer of metal (skin of an airplane) of various thicknesses. Their results showed that at atmospheric depths of 58 to 22 g/cm^2, thin metal shields (1 to 5 g/cm^2 of Fe) do not greatly affect the dose.

Armstrong et al. (ref. 5), using the compilations of Foelsche (as presented in ref. 6), have recently completed calculations of dose rates as a function of altitude for the upper and lower limits of the February 23, 1956, solar proton event. Their calculations include proton energies up to 3 GeV. As will be seen in "Results and Discussion," the results presented in reference 5 are higher by a factor of 2 to 3 than the average dose calculations presented herein. The calculations of reference 5 used maximum-dose conversion factors for normally incident neutrons and skin-dose conversion factors for normally incident protons. The two calculations agree within statistical accuracy when the same conversion factors are used (unpublished calculations of R. G. Alsmiller, Jr., Oak Ridge National Laboratory).

This paper presents spectrum-independent dose response functions for isotropically incident protons in the energy range 0.1 to 10 GeV as a function of altitude. By computing dose response rather than dose for a given spectrum, a single transport calculation gives all the response functions. These response functions can then be used to calculate dose for any number of arbitrary spectra within the energy range 0.1 to 10 GeV. Once the dose response functions are available, computations can be done in real time during a solar event. Thus, if the event spectrum can be measured, the altitude profile of dose rates can be predicted during the event. The shape of the curve of dose response function plotted against incident energy also indicates which measurements of the incident spectra are needed (that is, which energies are most important) for supersonic transport (SST) operations.

Also presented are the dose rates computed through the application of these response functions to several important solar proton events of solar cycle 19. Geomagnetic cutoffs have been incorporated by proper modification of the input spectra.

These response functions have been used previously by Foelsche et al. (ref. 6) to calculate dose rates in the upper atmosphere caused by the most important solar proton events of the last solar cycle and by galactic cosmic-ray protons. These calculations are compared with experimental results for galactic cosmic rays and discussed in reference 6.

SYMBOLS

$C_\gamma(E_\gamma)$	photon current-to-dose-rate conversion factor, $\frac{\text{rad}}{\text{photon/cm}^2}$
c	speed of light
D_γ	dose due to gamma rays (photons), rad
D_t	estimated total dose due to incident high-energy protons, rem or rad
E	energy, GeV
E_γ	photon energy, MeV
E_v	proton cutoff energy from vertical, GeV
E_w	proton cutoff energy from western horizon, GeV
f_γ	photon flux density, photons/cm^2-sec
$I(E,\lambda_{mag})$	transmission coefficient for protons of energy E at magnetic latitude λ_{mag} due to Earth's magnetic field, dimensionless
N	idealized exponential rigidity flux density of solar protons, protons/cm^2-hr
N_o	total flux density of solar protons, protons/cm^2-hr
P	proton rigidity, MV/c
P_o	rigidity parameter, MV/c
QF	quality factor, rem/rad
$R_n(E)$	dose response due to secondary neutrons produced by protons of energy E incident on top of atmosphere, $\frac{\text{rem or rad}}{\text{incident proton/cm}^2}$

$R_p(E)$ dose response due to primary and secondary protons from protons of energy E incident on top of atmosphere, $\frac{\text{rem or rad}}{\text{incident proton/cm}^2}$

$R_t(E)$ total dose response function due to protons of energy E incident on top of atmosphere, $\frac{\text{rem or rad}}{\text{incident proton/cm}^2}$

η_γ photon detector efficiency, counts/photon

λ_{mag} magnetic latitude, deg

$\Phi(E)$ proton fluence (through plane) incident on top of atmosphere, protons/cm^2-GeV

$\varphi_\gamma(E_\gamma)$ differential-energy flux density, photons/cm^2-sec-MeV

Ω solid angle, sr

METHOD OF CALCULATION

The Transport Code

The transport code is a set of computer programs written for the CDC 6600 computer. These programs record the history of each incident particle and its progeny until they are stopped, absorbed, or thermalized. An analysis program then reads the history tapes and compiles statistics on the fate of each generation of particles. For example, the statistics compiled for this study are differential-energy flux densities for neutrons and protons at various altitudes.

The transport program for energies below 400 MeV was written by Leimdorfer et al. and is described in reference 7. The basic structure of the Langley Research Center program is the same as that in reference 7. The Langley program is an extension to the GeV range and includes the transport of pions. This extension required nuclear-interaction data which were obtained as described in the following sections.

Range 0.75 to 2 GeV.- The nuclear-interaction data in this range were calculated by Bertini (ref. 8). Bertini's calculations of nuclear cross sections employ an intranuclear cascade in an impulse approximation. The impulse approximation assumes that the nucleus at all times during the interaction is composed only of nucleons (i.e., no exchange currents or resonances). The incident nucleons and resultant cascade nucleons are furthermore assumed to have only binary, or two-body, interactions, where the distributions of nucleons within the nucleus are taken from electromagnetic form factors.

Bertini assumed that pion production occurred through the $\left(\frac{3}{2}, \frac{3}{2}\right)$ resonance, where the decay, in the center-of-momentum system, was 50 percent isotropic, 25 percent forward, and 25 percent backward.

The proton-interaction data were taken from reference 8. This reference contains data for protons of energies 0.75, 1, and 2 GeV, and for neutrons of energy 1 GeV on the target elements O^{16}, Al^{27}, and Pb^{207}.

The neutron-interaction data within the same energy range were not available. The neutron data at energies of 0.75, 1, and 2 GeV on O^{16} were calculated for the present paper by using SU(2) symmetry and the proton data of reference 8. (Note that O^{16} has zero isotopic spin and is therefore a SU(2) scalar.) The cross sections, multiplicities, and energy-angle distributions found for neutrons (by using SU(2)) agreed to within 10 percent with the neutron data of reference 8 at 1 GeV. Thus, the interaction data for neutrons to 2 GeV were completed, and the Bertini calculations were shown to be consistent with this basic symmetry principle of strong interactions.

Range 2.0 to 10 GeV.- The range of energy for which nuclear interaction data are known (to 2 GeV) is not sufficient for solar events such as that which occurred on February 23, 1956, or especially for galactic cosmic rays. Since the experimental specific-yield functions for low-energy neutrons indicate that the energy dependence of primary protons in the GeV range only slightly affects the secondary nuclear yields in the upper atmosphere (ref. 9), the multiplicities and energy-angle distributions (normalized to the incident energy) were assumed not to change from 2 to 10 GeV. The pion component will, of course, not be correct at the higher energies since the onset of diffraction-production is ignored. Because energy is absorbed when pions are produced, the secondary nucleons will have a little less energy than the calculations predict. The pions are assumed not to have nuclear interactions since at high altitudes, their mean free path to decay is much smaller than their mean free path to nuclear interaction.

The transport calculations were carried out for 12 500 protons uniformly distributed over 25 incident-energy groups to cover the range 0.1 to 10 GeV. The final particle flux densities were compiled from approximately four million particle events, including those as many as 12 generations removed from the incident primary protons.

The Atmospheric Model

The thickness of the traversed layer in the atmosphere is expressed in units of g/cm^2. In this way the need for expressing explicitly the change of atmospheric density with depth is eliminated. Therefore, the model used for the atmosphere was considered to be an infinite layer of air of uniform density. The radiation was assumed to be isotropic (see ref. 10 for discussion) from the upper hemisphere.

The perturbation of the radiation field due to the presence of tissue and the airplane was neglected in the transport calculations. The length of the airplane, approximately 100 m, is small compared with the mean free path, which is greater than 1 km at SST cruising altitudes. Hence, because of the isotropy of the incident radiation and the large mean free path of protons and neutrons at even moderate energies, the penumbra formed will completely overcast the shadow of the entire airplane.

Dose Response Functions

Current-to-dose-rate conversion factors were used to transcribe flux densities obtained from the transport calculations to dose response. The conversion factors used were for a tissue composition of H^1, C^{12}, N^{14}, and O^{16}. Below 60 MeV, the factors for protons were calculated by assuming no nuclear interactions. The data for protons from 60 to 400 MeV were taken from Turner et al. (ref. 11). A simple energy-loss calculation indicates that the absorbed-dose conversion factors above 400 MeV can be assumed constant and equal to the absorbed-dose conversion factor of reference 11 at 400 MeV. The rem (dose equivalent) conversion above 400 MeV was found by using the average quality factor (ratio of rem to rad, see ref. 12) of 1.4 of Turner et al., which was computed at 400 MeV with nuclear interactions. The neutron current-to-dose-rate conversion factors were taken from Irving et al. (ref. 13) and Kinney and Zerby (ref. 14). All these conversion factors include the nuclear-star dose equivalent (nuclear interactions in tissue with multiple low-energy prongs) from protons and neutrons. The average- and skin-dose conversion factors for a 30-cm-thick slab of tissue for isotropic neutrons and protons were used in the present calculations. The extremity dose response functions were obtained by using the omnidirectional flux density and skin-dose conversion factors. (See ref. 6 for discussion.)

The contribution to the total dose due to particles other than nucleons (e.g., pions, electrons, and gammas) has been neglected. The absorbed dose (rad) will be too low by possibly as much as 30 percent but the dose equivalent (rem) will not be so greatly affected because of the low biological importance of these neglected radiations (that is, the quality factor $QF \approx 1$). For example, the dose from γ-rays produced by galactic cosmic rays, estimated from the measurements of Haymes (ref. 15) at the γ-transition maximum, is computed from

$$D_\gamma = \int C_\gamma(E_\gamma)\varphi_\gamma(E_\gamma)dE_\gamma$$

where C_γ is the photon current-to-dose-rate conversion factor and φ_γ is the photon differential-energy flux density. In magnitude

$$C_\gamma \leq 10^{-6} \frac{\text{mrad}}{\text{photon/cm}^2}$$

Define

$$f_\gamma \approx \int_{0.5\ \text{MeV}}^{3.5\ \text{MeV}} \varphi_\gamma(E_\gamma) dE_\gamma$$

where f_γ is known from reference 15 except for detector efficiency η_γ. Thus from reference 15, the photon flux density in the energy range 0.5 to 3.5 MeV is

$$f_\gamma = \frac{1.8 \times 10^3}{\eta_\gamma} \frac{\text{photons}}{\text{cm}^2\text{-hr}}$$

and the dose is overestimated by

$$D_\gamma \approx 10^{-6}\left(\frac{1.8 \times 10^3}{\eta_\gamma}\right) \frac{\text{mrad}}{\text{hr}} = \left(\frac{1.8 \times 10^{-3}}{\eta_\gamma}\right) \frac{\text{mrad}}{\text{hr}}$$

If η_γ is on the order of 10 percent, then

$$D_\gamma \leq 0.018 \frac{\text{mrad}}{\text{hr}}$$

This is on the order of 3 percent of the total absorbed dose, which was 0.65 mrad/hr. The dose due to γ-rays D_γ is only about 1 percent of the total dose equivalent (1.3 mrem/hr) at the same altitude. (See ref. 6.) Note that with η_γ = 10 percent, the total dose from γ-rays is on the order of 10 percent of the neutron absorbed dose rate (0.2 mrad/hr) of reference 6.

DOSE CALCULATION

Geomagnetic Cutoff

The normal geomagnetic-cutoff model can be represented by

$$I(E,\lambda_{mag}) = 1 - \exp(E_w - E)\Lambda(\lambda_{mag})$$

$$\Lambda(\lambda_{mag}) = \frac{0.693}{(E_v - E_w)}$$

where $I(E,\lambda_{mag})$ is the fraction of intensity transmitted at energy E, and E_v and E_w are the vertical and western cutoff energies, respectively, given in figure 1 (data taken

from ref. 16). This model does not account for the change in cutoff due to depression of the earth's magnetic field by solar cosmic rays, a situation which oftens occurs during periods of high solar activity. This change in cutoff has not been included since it is as yet a not too well understood phenomenon.

Dose Integral

With the dose response functions, the dose averaged over the body or the dose in extremities is easily calculated when the incident spectra are known. The dose at high latitudes $\lambda_{mag} \gtrsim 68^{o}$ is given by

$$D_t = \int_{0.1\ GeV}^{10\ GeV} R_t(E)\ \Phi(E)dE$$

where $R_t(E)$ is the corresponding dose response function and Φ is the incident proton fluence through a plane* in protons/cm^2-GeV. To include latitude effects, then

$$D_t(\lambda_{mag}) = \int_{0.1}^{10\ GeV} R_t(E)I(E,\lambda_{mag})\Phi(E)dE$$

where $I(E,\lambda_{mag})$ is the transmission at geomagnetic latitude λ_{mag} and was given in the previous section.

RESULTS AND DISCUSSION

The dose response functions for dose averaged over the body and for extremities are shown for altitudes from 300 to 20 g/cm^2 in figures 2 to 7. These curves were obtained by smoothing the Monte Carlo data given in tables I to VI. The greatest statistical fluctuations were at the lower incident energies of the proton dose response functions (figs. 2 and 5), where the curves are falling by orders of magnitude. The neutron dose response had, in general, considerably less statistical scatter than that of protons. This is due to the much larger number of neutrons, which provides a larger statistical sample. The slight depression in dose at 0.4 GeV as seen in the tables is due to the fact that two different transport codes joined the data at 0.4 GeV. These codes usually give slightly different results at the energy where they are combined.

At altitudes for subsonic flight (about 300 g/cm^2) no significant dose is generally expected. At the present SST cruising altitudes of 19.8 km (about 58 g/cm^2), moderate

---

*Fluence through a plane = $\frac{1}{2}$ fluence through a sphere:

Φ protons/cm^2-GeV = $\frac{1}{2}\ 2\pi$ sr $\frac{d\Phi}{d\Omega}$ protons/cm^2-GeV-sr.

radiation doses are expected from solar events with energies above 0.25 GeV. At cruising altitudes of 20 g/cm^2, virtually all solar events (except the low-energy events $E \lesssim 0.1$ GeV) have potential for producing a significant dose. This is particularly true for the extremity dose at 20 g/cm^2 as seen in figures 5 and 7. The peak in the dose response function (Bragg peak) is due to uncollided primary protons. This peak does not occur at the lower altitudes shown in the figures since nearly all primary protons have suffered at least one nuclear interaction.

The surface dose as calculated in reference 1 is presented in figure 8 in comparison with the extremity dose of the present work for rigidities of 150, 250, and 350 MV/c. The greatest differences at lower altitudes are presumably due to the simplified nuclear interaction model used in reference 1; in this model the incident energy at interaction was assumed to be equally shared among all secondary particles.

The presently calculated average doses are compared in figure 9 with the results of reference 3 for a rigidity spectrum with $P_o = 100$ MV/c. The absorbed dose (rad) of reference 3 is in good agreement with the present calculations; however, at lower altitudes the dose equivalent (rem) is different. This indicates some discrepancies in the calculation of dose for neutrons in the two calculations.

Spectra for two solar events of cycle 19 are shown in figure 10 as compiled by Foelsche from measured data (ref. 6). The prompt spectra of the February 23, 1956, event were observed on different locations during the maximum phase of the event in the first hours after particle onset. The spectra of the November 12, 1960, event were observed 5 hours (1840 UT), 10 hours (2330 UT), and 27 hours (1603 UT on Nov. 13) after the particle onset. Extensive results (for whole-body average dose rates) of the present calculations applied to these spectra can be found in reference 6.

The extremity dose rates for the upper and lower limits of the February 23, 1956, event are shown in figure 11 along with similar calculations from reference 5. In reference 5, the spectra were cut off above 3 GeV and the conversion factors used were skin dose for protons and maximum dose for neutrons. Although the transport calculations were for protons isotropically incident at the top of the atmosphere, the conversion factors used in reference 5 were for neutrons and protons normally incident on the tissue sample. The agreement of the two results is reasonably good, especially for the lower limit to the February 1956 event. The average dose rate for the same event as presented in reference 6 is lower by a factor of 2 to 3 than the extremity dose rates of the present calculations and the dose rates of reference 5. When the same conversion factors are used and the primary spectra are cut off at 3 GeV, the calculations of reference 5 and the present calculations are in complete agreement. The average and extremity dose rates during the November 12, 1960, event are shown in figures 12 and 13. This event is characteristic of medium-energy, high-intensity solar events.

CONCLUDING REMARKS

The importance of the dose response functions with respect to the supersonic transport (SST) is twofold. First, they have been used by Foelsche et al. to assess theoretically the radiation hazard to the SST. There is, of course, the need for experimental verification of these results. Second, with the response functions presented herein and with sufficient real-time measurements by both satellite and by ground-based neutron monitors, it is possible that current estimates of extremity and depth dose rates can be given so that SST flights may be rescheduled, or evasive measures can be taken to minimize exposure.

Langley Research Center,
National Aeronautics and Space Administration,
Hampton, Va., October 2, 1970.

REFERENCES

1. Flamm, E. J.; and Lingenfelter, R. E.: Neutron and Proton Dosages in the Upper Atmosphere From Solar Flare Radiation. Science, vol. 144, no. 3626, June 26, 1964, pp. 1566-1569.

2. Engelmann, J.; Hautdidier, A.; and Koch, L.: Energy Spectra and Time Profile of Protons Emitted During the Solar Flare of June 9, 1968. 11th International Conference on Cosmic Rays (Budapest), [1969]. (Available from CFSTI.)

3. Leimdorfer, M.; Alsmiller, R. G., Jr.; and Boughner, R. T.: Calculations of the Radiation Hazard Due to Exposure of Supersonic Aircraft to Solar-Flare Protons. Nucl. Sci. Eng., vol. 27, no. 1, Jan. 1967, pp. 151-157.

4. Bertini, Hugo W.: Low-Energy Intranuclear Cascade Calculation. Phys. Rev., Second Ser., vol. 131, no. 4, Aug. 15, 1963, pp. 1801-1821.

5. Armstrong, T. W.; Alsmiller, R. G.; and Barish, J.: Calculation of the Radiation Hazard at Supersonic Aircraft Altitudes Produced by an Energetic Solar Flare. Nucl. Sci. Eng., vol. 37, no. 3, Sept. 1969, pp. 337-342.

6. Foelsche, T.; Mendell, Rosalind; Adams, Richard R.; and Wilson, John W.: Measured and Calculated Radiation Levels Produced by Galactic and Solar Cosmic Rays in SST Altitudes and Precaution Measures to Minimize Implications at Commercial SST-Operations. NASA paper presented at French-Anglo United States Supersonic Transport Meeting (Paris, France), Mar. 3, 1969.

7. Leimdorfer, Martin; and Crawford, George W., eds.: Penetration and Interaction of Protons With Matter – Pt. I. Theoretical Studies Using Monte Carlo Techniques. Res. Rep. No. 68-2 (Grant NsG 708), Southern Methodist Univ., Aug. 1968.

8. Bertini, Hugo W.: Preliminary Data From Intranuclear-Cascade Calculations of 0.75-, 1-, and 2-GeV Protons on Oxygen, Aluminum, and Lead, and 1-GeV Neutrons on the Same Elements. ORNL-TM-1966, U. S. At. Energy Comm., Dec. 1967.

9. Good, Robert C., Jr.: Atmospheric Transition Curves for Geomagnetically-Sensitive Cosmic Rays. NASA CR-66110, 1966.

10. McCracken, Kenneth G.: Anisotropies in Cosmic Radiation of Solar Origin. Solar Proton Manual, Frank B. McDonald, ed., NASA TR R-169, 1963, pp. 57-88.

11. Turner, J. E.; Zerby, C. D.; Woodyard, R. L.; Wright, H. A.; Kinney, W. E.; Snyder, W. S.; and Neufeld, J.: Calculation of Radiation Dose From Protons to 400 MeV. Health Phys., vol. 10, no. 11, Nov. 1964, pp. 783-808.

12. Trubey, D. K.: Use of ICRU-Defined Quantities and Units in Shielding. ORNL-RSIC-16, U.S. At. Energy Comm., Oct 1968.

13. Irving, D. C.; Alsmiller, R. G.; and Moran, H. S.: Tissue Current-to-Dose Conversion Factors for Neutrons With Energies From 0.5 to 60 MeV. ORNL-4032, U.S. At. Energy Comm., Aug. 1967.

14. Kinney, W. E.; and Zerby, C. D.: Calculated Tissue Current-to-Dose Conversion Factors for Nucleons of Energy Below 400 MeV. Second Symposium on Protection Against Radiations in Space, NASA SP-71, 1965, pp. 161-172.

15. Haymes, Robert C.: Fast Neutrons in the Earth's Atmosphere – 1. Variation With Depth. J. Geophys. Res. vol. 69, no. 5, Mar. 1, 1964, pp. 841-852.

16. Lemaitre, G.; and Vallarta, M. S.: On the Allowed Cone of Cosmic Radiation. Phys. Rev., Second Ser., vol. 50, no. 6, Sept. 15, 1936, pp. 493-504.

TABLE I.- PROTON AVERAGE DOSE RESPONSE FUNCTIONS

DUE TO INCIDENT PROTONS

Energy range, GeV	20 g/cm^2	58 g/cm^2	100 g/cm^2	200 g/cm^2	300 g/cm^2
	Dose response function, $\frac{\text{rad}}{\text{incident proton/cm}^2}$				
.10-.15	0.	0.	0.	0.	0.
.15-.20	2.75E-09	0.	0.	0.	0.
.20-.25	1.78E-08	5.19E-11	0.	0.	0.
.25-.30	3.38E-08	1.04E-10	0.	0.	0.
.30-.35	5.21E-08	2.01E-09	0.	0.	0.
.35-.40	6.05E-08	1.16E-08	1.04E-10	0.	0.
.40-.50	4.02E-08	1.37E-08	1.78E-09	0.	0.
.50-.60	7.88E-08	3.68E-08	1.16E-08	0.	0.
.60-.70	8.80E-08	4.78E-08	2.32E-08	4.93E-10	0.
.70-.80	8.76E-08	4.86E-08	2.91E-08	3.04E-09	1.95E-10
.80-.90	9.35E-08	5.67E-08	2.99E-08	6.30E-09	4.81E-10
.90-1.0	9.24E-08	5.68E-08	3.71E-08	1.02E-08	1.02E-09
1.0-1.5	9.94E-08	6.72E-08	4.32E-08	1.70E-08	5.21E-09
1.5-2.0	1.09E-07	8.33E-08	6.03E-08	2.70E-08	1.01E-08
2.0-2.5	1.12E-07	8.32E-08	6.32E-08	2.76E-08	1.24E-08
2.5-3.0	1.19E-07	9.35E-08	7.23E-08	3.76E-08	1.67E-08
3.0-3.5	1.27E-07	1.13E-07	8.33E-08	4.04E-08	2.23E-08
3.5-4.0	1.40E-07	1.07E-07	9.22E-08	5.49E-08	2.81E-08
4.0-4.5	1.45E-07	1.32E-07	1.05E-07	6.22E-08	2.83E-08
4.5-5.0	1.62E-07	1.47E-07	1.15E-07	6.09E-08	3.35E-08
5.0-6.0	1.68E-07	1.51E-07	1.23E-07	7.58E-08	3.71E-08
6.0-7.0	1.88E-07	1.72E-07	1.39E-07	9.19E-08	4.95E-08
7.0-8.0	1.94E-07	1.86E-07	1.71E-07	1.05E-07	5.84E-08
8.0-9.0	2.10E-07	2.02E-07	1.62E-07	1.25E-07	6.88E-08
9.0-10.0	2.41E-07	2.31E-07	2.05E-07	1.17E-07	7.26E-08
	Dose response function, $\frac{\text{rem}}{\text{incident proton/cm}^2}$				
.10-.15	0.	0.	0.	0.	0.
.15-.20	3.99E-09	0.	0.	0.	0.
.20-.25	2.54E-08	7.52E-11	0.	0.	0.
.25-.30	4.69E-08	1.50E-10	0.	0.	0.
.30-.35	6.90E-08	2.89E-09	0.	0.	0.
.35-.40	8.10E-08	1.64E-08	1.50E-10	0.	0.
.40-.50	5.59E-08	1.84E-08	2.53E-09	0.	0.
.50-.60	1.11E-07	5.09E-08	1.59E-08	0.	0.
.60-.70	1.24E-07	6.68E-08	3.22E-08	7.06E-10	0.
.70-.80	1.24E-07	6.86E-08	4.07E-08	4.20E-09	2.78E-10
.80-.90	1.33E-07	8.01E-08	4.19E-08	8.66E-09	6.83E-10
.90-1.0	1.31E-07	8.02E-08	5.21E-08	1.43E-08	1.40E-09
1.0-1.5	1.41E-07	9.46E-08	6.07E-08	2.36E-08	7.31E-09
1.5-2.0	1.55E-07	1.18E-07	8.50E-08	3.81E-08	1.38E-08
2.0-2.5	1.58E-07	1.17E-07	8.91E-08	3.87E-08	1.74E-08
2.5-3.0	1.68E-07	1.32E-07	1.02E-07	5.28E-08	2.33E-08
3.0-3.5	1.80E-07	1.59E-07	1.17E-07	5.67E-08	3.14E-08
3.5-4.0	1.98E-07	1.51E-07	1.30E-07	7.72E-08	3.92E-08
4.0-4.5	2.06E-07	1.86E-07	1.48E-07	8.72E-08	3.93E-08
4.5-5.0	2.28E-07	2.07E-07	1.62E-07	8.58E-08	4.69E-08
5.0-6.0	2.38E-07	2.12E-07	1.73E-07	1.07E-07	5.17E-08
6.0-7.0	2.66E-07	2.42E-07	1.96E-07	1.29E-07	6.91E-08
7.0-8.0	2.74E-07	2.62E-07	2.40E-07	1.47E-07	8.18E-08
8.0-9.0	2.96E-07	2.84E-07	2.29E-07	1.75E-07	9.66E-08
9.0-10.0	3.40E-07	3.25E-07	2.88E-07	1.65E-07	1.02E-07

TABLE II.- NEUTRON AVERAGE DOSE RESPONSE FUNCTIONS

DUE TO INCIDENT PROTONS

Energy range, GeV	20 g/cm^2	58 g/cm^2	100 g/cm^2	200 g/cm^2	300 g/cm^2
	Dose response function, $\frac{\text{rad}}{\text{incident proton/cm}^2}$				
.10-.15	6.21E-10	3.83E-10	1.70E-10	0.	0.
.15-.20	1.00E-09	4.40E-10	1.99E-10	5.00E-11	0.
.20-.25	1.64E-09	1.02E-09	6.96E-10	2.44E-10	8.62E-11
.25-.30	2.31E-09	1.40E-09	7.83E-10	2.33E-10	1.05E-10
.30-.35	2.77E-09	2.45E-09	1.51E-09	3.89E-10	1.63E-10
.35-.40	3.74E-09	3.16E-09	2.07E-09	6.13E-10	1.63E-10
.40-.50	3.24E-09	3.11E-09	2.24E-09	7.70E-10	2.63E-10
.50-.60	8.36E-09	8.61E-09	6.46E-09	2.71E-09	1.14E-09
.60-.70	9.58E-09	1.10E-08	8.61E-09	4.00E-09	1.65E-09
.70-.80	1.22E-08	1.45E-08	1.21E-08	5.75E-09	2.46E-09
.80-.90	1.27E-08	1.51E-08	1.46E-08	7.80E-09	3.81E-09
.90-1.0	1.46E-08	1.59E-08	1.57E-08	9.93E-09	4.95E-09
1.0-1.5	1.81E-08	2.16E-08	1.99E-08	1.27E-08	7.15E-09
1.5-2.0	2.25E-08	2.56E-08	2.51E-08	1.79E-08	1.17E-08
2.0-2.5	2.73E-08	3.25E-08	3.20E-08	2.41E-08	1.34E-08
2.5-3.0	3.03E-08	3.73E-08	3.67E-08	2.83E-08	1.78E-08
3.0-3.5	3.82E-08	4.49E-08	4.39E-08	3.28E-08	2.25E-08
3.5-4.0	3.81E-08	4.57E-08	4.63E-08	3.76E-08	2.62E-08
4.0-4.5	4.18E-08	5.42E-08	5.45E-08	4.32E-08	2.92E-08
4.5-5.0	4.73E-08	5.98E-08	5.89E-08	4.68E-08	2.94E-08
5.0-6.0	5.42E-08	6.51E-08	6.66E-08	5.43E-08	3.65E-08
6.0-7.0	6.22E-08	7.82E-08	7.91E-08	6.42E-08	4.56E-08
7.0-8.0	7.10E-08	8.94E-08	9.08E-08	7.28E-08	4.99E-08
8.0-9.0	8.16E-08	9.69E-08	1.02E-07	8.44E-08	6.01E-08
9.0-10.0	8.77E-08	1.10E-07	1.13E-07	9.26E-08	6.17E-08
	Dose response function, $\frac{\text{rem}}{\text{incident proton/cm}^2}$				
.10-.15	4.00E-09	2.45E-09	1.10E-09	0.	0.
.15-.20	6.11E-09	2.59E-09	1.07E-09	2.79E-10	0.
.20-.25	9.32E-09	5.74E-09	3.79E-09	1.29E-09	4.53E-10
.25-.30	1.27E-08	7.75E-09	4.38E-09	1.29E-09	6.12E-10
.30-.35	1.47E-08	1.30E-08	8.24E-09	2.31E-09	9.72E-10
.35-.40	1.95E-08	1.67E-08	1.06E-08	3.18E-09	6.85E-10
.40-.50	1.50E-08	1.56E-08	1.14E-08	3.72E-09	1.21E-09
.50-.60	4.00E-08	4.04E-08	3.04E-08	1.33E-08	5.68E-09
.60-.70	4.71E-08	5.19E-08	4.00E-08	1.99E-08	8.39E-09
.70-.80	6.02E-08	7.01E-08	5.98E-08	2.64E-08	1.16E-08
.80-.90	6.35E-08	7.26E-08	6.79E-08	3.68E-08	1.89E-08
.90-1.0	7.41E-08	7.73E-08	7.39E-08	4.66E-08	2.26E-08
1.0-1.5	9.37E-08	1.06E-07	9.66E-08	6.02E-08	3.46E-08
1.5-2.0	1.19E-07	1.31E-07	1.26E-07	8.51E-08	5.67E-08
2.0-2.5	1.41E-07	1.65E-07	1.59E-07	1.16E-07	6.39E-08
2.5-3.0	1.58E-07	1.90E-07	1.85E-07	1.36E-07	8.64E-08
3.0-3.5	2.03E-07	2.28E-07	2.19E-07	1.61E-07	1.10E-07
3.5-4.0	1.95E-07	2.32E-07	2.30E-07	1.83E-07	1.23E-07
4.0-4.5	2.19E-07	2.73E-07	2.69E-07	2.09E-07	1.42E-07
4.5-5.0	2.41E-07	2.99E-07	2.92E-07	2.33E-07	1.45E-07
5.0-6.0	2.78E-07	3.31E-07	3.35E-07	2.65E-07	1.76E-07
6.0-7.0	3.17E-07	3.97E-07	3.94E-07	3.11E-07	2.17E-07
7.0-8.0	3.61E-07	4.52E-07	4.51E-07	3.57E-07	2.44E-07
8.0-9.0	4.15E-07	4.86E-07	5.09E-07	4.04E-07	2.87E-07
9.0-10.0	4.45E-07	5.52E-07	5.56E-07	4.51E-07	2.96E-07

TABLE III.- TOTAL AVERAGE DOSE RESPONSE FUNCTIONS

DUE TO INCIDENT PROTONS

Energy range, GeV	20 g/cm^2	58 g/cm^2	100 g/cm^2	200 g/cm^2	300 g/cm^2
	Dose response function, $\frac{\text{rad}}{\text{incident proton/cm}^2}$				
.10-.15	6.21E-10	3.83E-10	1.70E-10	0.	0.
.15-.20	3.75E-09	4.40E-10	1.99E-10	5.00E-11	0.
.20-.25	1.95E-08	1.07E-09	6.96E-10	2.44E-10	8.62E-11
.25-.30	3.61E-08	1.50E-09	7.83E-10	2.33E-10	1.05E-10
.30-.35	5.49E-08	4.46E-09	1.51E-09	3.89E-10	1.63E-10
.35-.40	6.43E-08	1.48E-08	2.18E-09	6.13E-10	1.63E-10
.40-.50	4.34E-08	1.69E-08	4.02E-09	7.70E-10	2.63E-10
.50-.60	8.72E-08	4.54E-08	1.81E-08	2.71E-09	1.14E-09
.60-.70	9.75E-08	5.88E-08	3.18E-08	4.49E-09	1.65E-09
.70-.80	9.98E-08	6.32E-08	4.12E-08	8.79E-09	2.65E-09
.80-.90	1.06E-07	7.19E-08	4.45E-08	1.41E-08	4.29E-09
.90-1.0	1.07E-07	7.27E-08	5.28E-08	2.02E-08	5.97E-09
1.0-1.5	1.18E-07	8.88E-08	6.31E-08	2.96E-08	1.24E-08
1.5-2.0	1.32E-07	1.09E-07	8.54E-08	4.50E-08	2.17E-08
2.0-2.5	1.39E-07	1.16E-07	9.52E-08	5.16E-08	2.58E-08
2.5-3.0	1.49E-07	1.31E-07	1.09E-07	6.59E-08	3.45E-08
3.0-3.5	1.66E-07	1.58E-07	1.27E-07	7.32E-08	4.48E-08
3.5-4.0	1.78E-07	1.53E-07	1.38E-07	9.25E-08	5.43E-08
4.0-4.5	1.87E-07	1.86E-07	1.60E-07	1.05E-07	5.75E-08
4.5-5.0	2.09E-07	2.07E-07	1.74E-07	1.08E-07	6.29E-08
5.0-6.0	2.22E-07	2.16E-07	1.90E-07	1.30E-07	7.36E-08
6.0-7.0	2.50E-07	2.50E-07	2.18E-07	1.56E-07	9.51E-08
7.0-8.0	2.65E-07	2.75E-07	2.62E-07	1.77E-07	1.08E-07
8.0-9.0	2.91E-07	2.99E-07	2.64E-07	2.09E-07	1.29E-07
9.0-10.0	3.29E-07	3.41E-07	3.17E-07	2.10E-07	1.34E-07
	Dose response function, $\frac{\text{rem}}{\text{incident proton/cm}^2}$				
.10-.15	4.00E-09	2.45E-09	1.10E-09	0.	0.
.15-.20	1.01E-08	2.59E-09	1.07E-09	2.79E-10	0.
.20-.25	3.47E-08	5.81E-09	3.79E-09	1.29E-09	4.53E-10
.25-.30	5.95E-08	7.90E-09	4.38E-09	1.29E-09	6.12E-10
.30-.35	8.37E-08	1.59E-08	8.24E-09	2.31E-09	9.72E-10
.35-.40	1.00E-07	3.30E-08	1.08E-08	3.18E-09	6.85E-10
.40-.50	7.09E-08	3.40E-08	1.40E-08	3.72E-09	1.21E-09
.50-.60	1.51E-07	9.14E-08	4.62E-08	1.33E-08	5.68E-09
.60-.70	1.72E-07	1.19E-07	7.22E-08	2.06E-08	8.39E-09
.70-.80	1.84E-07	1.39E-07	1.00E-07	3.06E-08	1.19E-08
.80-.90	1.96E-07	1.53E-07	1.10E-07	4.54E-08	1.96E-08
.90-1.0	2.05E-07	1.58E-07	1.26E-07	6.08E-08	2.40E-08
1.0-1.5	2.35E-07	2.01E-07	1.57E-07	8.38E-08	4.19E-08
1.5-2.0	2.74E-07	2.49E-07	2.11E-07	1.23E-07	7.04E-08
2.0-2.5	2.99E-07	2.83E-07	2.48E-07	1.55E-07	8.12E-08
2.5-3.0	3.26E-07	3.22E-07	2.87E-07	1.89E-07	1.10E-07
3.0-3.5	3.83E-07	3.87E-07	3.36E-07	2.18E-07	1.41E-07
3.5-4.0	3.93E-07	3.83E-07	3.61E-07	2.60E-07	1.62E-07
4.0-4.5	4.25E-07	4.59E-07	4.17E-07	2.96E-07	1.82E-07
4.5-5.0	4.69E-07	5.06E-07	4.54E-07	3.18E-07	1.92E-07
5.0-6.0	5.16E-07	5.43E-07	5.08E-07	3.71E-07	2.28E-07
6.0-7.0	5.83E-07	6.39E-07	5.90E-07	4.40E-07	2.86E-07
7.0-8.0	6.35E-07	7.14E-07	6.91E-07	5.04E-07	3.26E-07
8.0-9.0	7.11E-07	7.71E-07	7.38E-07	5.80E-07	3.83E-07
9.0-10.0	7.86E-07	8.77E-07	8.44E-07	6.16E-07	3.98E-07

TABLE IV.- PROTON EXTREMITY DOSE RESPONSE FUNCTIONS DUE TO INCIDENT PROTONS

Energy range, GeV	20 g/cm^2	58 g/cm^2	100 g/cm^2	200 g/cm^2	300 g/cm^2
	Dose response function, $\frac{\text{rad}}{\text{incident proton/cm}^2}$				
.10-.15	0.	0.	0.	0.	0.
.15-.20	9.40E-08	0.	0.	0.	0.
.20-.25	1.54E-07	1.77E-09	0.	0.	0.
.25-.30	1.46E-07	3.55E-09	0.	0.	0.
.30-.35	1.38E-07	4.64E-08	0.	0.	0.
.35-.40	1.20E-07	7.87E-08	3.55E-09	0.	0.
.40-.50	6.84E-08	4.29E-08	1.16E-08	0.	0.
.50-.60	1.46E-07	9.13E-08	5.16E-08	0.	0.
.60-.70	1.56E-07	1.06E-07	5.70E-08	7.92E-09	0.
.70-.80	1.65E-07	1.08E-07	6.66E-08	1.14E-08	2.19E-09
.80-.90	1.66E-07	1.11E-07	6.97E-08	2.38E-08	3.01E-09
.90-1.0	1.80E-07	1.13E-07	9.26E-08	3.92E-08	7.09E-09
1.0-1.5	1.82E-07	1.39E-07	9.97E-08	4.48E-08	1.35E-08
1.5-2.0	2.26E-07	1.87E-07	1.20E-07	6.29E-08	2.63E-08
2.0-2.5	2.78E-07	1.92E-07	1.47E-07	7.52E-08	4.70E-08
2.5-3.0	2.78E-07	2.34E-07	1.70E-07	1.01E-07	4.42E-08
3.0-3.5	3.07E-07	2.70E-07	2.36E-07	1.17E-07	7.13E-08
3.5-4.0	3.22E-07	2.89E-07	2.58E-07	1.68E-07	1.01E-07
4.0-4.5	3.90E-07	3.36E-07	2.69E-07	1.79E-07	6.69E-08
4.5-5.0	4.05E-07	3.87E-07	3.12E-07	1.75E-07	1.07E-07
5.0-6.0	4.07E-07	3.95E-07	3.22E-07	2.37E-07	1.15E-07
6.0-7.0	5.17E-07	4.65E-07	3.89E-07	2.59E-07	1.36E-07
7.0-8.0	5.19E-07	5.21E-07	4.95E-07	2.96E-07	1.92E-07
8.0-9.0	5.50E-07	6.06E-07	4.62E-07	3.27E-07	1.92E-07
9.0-10.0	6.50E-07	6.44E-07	5.88E-07	3.28E-07	2.26E-07
	Dose response function, $\frac{\text{rem}}{\text{incident proton/cm}^2}$				
.10-.15	0.	0.	0.	0.	0.
.15-.20	2.29E-07	0.	0.	0.	0.
.20-.25	3.21E-07	4.32E-09	0.	0.	0.
.25-.30	2.58E-07	8.64E-09	0.	0.	0.
.30-.35	2.40E-07	1.10E-07	0.	0.	0.
.35-.40	2.03E-07	1.58E-07	8.64E-09	0.	0.
.40-.50	1.16E-07	8.19E-08	2.26E-08	0.	0.
.50-.60	2.60E-07	1.68E-07	1.02E-07	0.	0.
.60-.70	2.74E-07	1.97E-07	1.00E-07	1.82E-08	0.
.70-.80	2.95E-07	2.04E-07	1.20E-07	2.04E-08	4.80E-09
.80-.90	2.86E-07	1.93E-07	1.30E-07	4.69E-08	5.77E-09
.90-1.0	3.24E-07	2.03E-07	1.74E-07	7.66E-08	1.51E-08
1.0-1.5	3.22E-07	2.53E-07	1.89E-07	8.50E-08	2.58E-08
1.5-2.0	4.13E-07	3.46E-07	2.14E-07	1.15E-07	4.84E-08
2.0-2.5	5.34E-07	3.56E-07	2.72E-07	1.45E-07	9.54E-08
2.5-3.0	5.29E-07	4.46E-07	3.19E-07	1.93E-07	8.18E-08
3.0-3.5	5.83E-07	5.10E-07	4.63E-07	2.33E-07	1.39E-07
3.5-4.0	5.03E-07	5.61E-07	5.02E-07	3.33E-07	2.09E-07
4.0-4.5	7.66E-07	6.40E-07	5.13E-07	3.50E-07	1.22E-07
4.5-5.0	7.69E-07	7.50E-07	6.04E-07	3.43E-07	2.12E-07
5.0-6.0	7.68E-07	7.57E-07	6.11E-07	4.72E-07	2.30E-07
6.0-7.0	1.01E-06	8.99E-07	7.57E-07	4.98E-07	2.59E-07
7.0-8.0	1.01E-06	1.02E-06	9.72E-07	5.76E-07	3.82E-07
8.0-9.0	1.06E-06	1.20E-06	9.07E-07	6.25E-07	3.76E-07
9.0-10.0	1.25E-06	1.25E-06	1.14E-06	6.33E-07	4.49E-07

TABLE V.- NEUTRON EXTREMITY DOSE RESPONSE FUNCTIONS

DUE TO INCIDENT PROTONS

Energy range, GeV	20 g/cm^2	58 g/cm^2	100 g/cm^2	200 g/cm^2	300 g/cm^2
	Dose response function, $\frac{\text{rad}}{\text{incident proton/cm}^2}$				
.10-.15	1.29E-09	7.71E-10	2.81E-10	0.	0.
.15-.20	2.72E-09	1.03E-09	4.95E-10	4.86E-11	0.
.20-.25	3.91E-09	2.36E-09	1.16E-09	4.50E-10	1.90E-10
.25-.30	5.94E-09	3.14E-09	1.54E-09	6.12E-10	2.35E-10
.30-.35	6.18E-09	4.57E-09	2.36E-09	9.89E-10	4.23E-10
.35-.40	8.52E-09	6.17E-09	3.36E-09	1.21E-09	1.97E-10
.40-.50	5.66E-09	6.14E-09	4.25E-09	1.30E-09	3.62E-10
.50-.60	1.70E-08	1.61E-08	1.13E-08	3.84E-09	1.97E-09
.60-.70	1.93E-08	2.06E-08	1.49E-08	6.42E-09	2.60E-09
.70-.80	2.52E-08	2.72E-08	2.31E-08	9.91E-09	3.69E-09
.80-.90	2.83E-08	2.98E-08	2.58E-08	1.27E-08	6.11E-09
.90-1.0	3.29E-08	3.32E-08	2.91E-08	1.59E-08	7.63E-09
1.0-1.5	4.09E-08	4.59E-08	3.98E-08	2.09E-08	1.13E-08
1.5-2.0	5.57E-08	5.90E-08	5.42E-08	3.05E-08	2.09E-08
2.0-2.5	6.30E-08	7.18E-08	6.51E-08	4.40E-08	2.25E-08
2.5-3.0	7.06E-08	8.54E-08	7.69E-08	5.14E-08	3.19E-08
3.0-3.5	8.64E-08	1.03E-07	9.45E-08	6.23E-08	3.98E-08
3.5-4.0	8.47E-08	1.01E-07	1.00E-07	7.10E-08	4.16E-08
4.0-4.5	9.73E-08	1.21E-07	1.14E-07	8.15E-08	5.29E-08
4.5-5.0	1.04E-07	1.32E-07	1.30E-07	8.97E-08	5.29E-08
5.0-6.0	1.20E-07	1.46E-07	1.41E-07	1.03E-07	6.62E-08
6.0-7.0	1.32E-07	1.72E-07	1.67E-07	1.16E-07	7.69E-08
7.0-8.0	1.53E-07	1.99E-07	1.85E-07	1.35E-07	9.40E-08
8.0-9.0	1.81E-07	2.15E-07	2.14E-07	1.57E-07	1.01E-07
9.0-10.0	1.88E-07	2.35E-07	2.33E-07	1.77E-07	1.12E-07
	Dose response function, $\frac{\text{rem}}{\text{incident proton/cm}^2}$				
.10-.15	6.45E-09	3.87E-09	1.41E-09	0.	0.
.15-.20	1.36E-08	5.18E-09	2.48E-09	2.43E-10	0.
.20-.25	1.96E-08	1.18E-08	5.83E-09	2.26E-09	9.51E-10
.25-.30	2.98E-08	1.57E-08	7.70E-09	3.07E-09	1.18E-09
.30-.35	3.10E-08	2.29E-08	1.18E-08	4.96E-09	2.12E-09
.35-.40	4.27E-08	3.09E-08	1.68E-08	6.09E-09	9.87E-10
.40-.50	2.84E-08	3.08E-08	2.13E-08	6.52E-09	1.81E-09
.50-.60	8.52E-08	8.09E-08	5.68E-08	1.93E-08	9.90E-09
.60-.70	9.69E-08	1.03E-07	7.44E-08	3.22E-08	1.31E-08
.70-.80	1.26E-07	1.36E-07	1.16E-07	4.97E-08	1.85E-08
.80-.90	1.42E-07	1.49E-07	1.29E-07	6.35E-08	3.06E-08
.90-1.0	1.65E-07	1.66E-07	1.46E-07	7.95E-08	3.82E-08
1.0-1.5	2.05E-07	2.30E-07	2.00E-07	1.05E-07	5.64E-08
1.5-2.0	2.79E-07	2.96E-07	2.72E-07	1.53E-07	1.05E-07
2.0-2.5	3.16E-07	3.60E-07	3.26E-07	2.21E-07	1.13E-07
2.5-3.0	3.54E-07	4.28E-07	3.85E-07	2.58E-07	1.60E-07
3.0-3.5	4.33E-07	5.15E-07	4.74E-07	3.12E-07	1.99E-07
3.5-4.0	4.25E-07	5.08E-07	5.01E-07	3.56E-07	2.09E-07
4.0-4.5	4.88E-07	6.07E-07	5.71E-07	4.09E-07	2.65E-07
4.5-5.0	5.21E-07	6.63E-07	6.50E-07	4.50E-07	2.65E-07
5.0-6.0	6.03E-07	7.31E-07	7.06E-07	5.16E-07	3.32E-07
6.0-7.0	6.61E-07	8.61E-07	8.39E-07	5.82E-07	3.85E-07
7.0-8.0	7.69E-07	9.99E-07	9.25E-07	6.76E-07	4.71E-07
8.0-9.0	9.06E-07	1.08E-06	1.07E-06	7.86E-07	5.08E-07
9.0-10.0	9.42E-07	1.18E-06	1.17E-06	8.89E-07	5.63E-07

TABLE VI.- TOTAL EXTREMITY DOSE RESPONSE FUNCTIONS

DUE TO INCIDENT PROTONS

Energy range, GeV	20 g/cm^2	58 g/cm^2	100 g/cm^2	200 g/cm^2	300 g/cm^2
	Dose response function, $\frac{\text{rad}}{\text{incident proton/cm}^2}$				
.10-.15	1.29E-09	7.71E-10	2.81E-10	0.	0.
.15-.20	9.68E-08	1.03E-09	4.95E-10	4.86E-11	0.
.20-.25	1.58E-07	4.13E-09	1.16E-09	4.50E-10	1.90E-10
.25-.30	1.52E-07	6.69E-09	1.54E-09	6.12E-10	2.35E-10
.30-.35	1.44E-07	5.10E-08	2.36E-09	9.89E-10	4.23E-10
.35-.40	1.29E-07	8.49E-08	6.91E-09	1.21E-09	1.97E-10
.40-.50	7.41E-08	4.90E-08	1.59E-08	1.30E-09	3.62E-10
.50-.60	1.63E-07	1.07E-07	6.30E-08	3.84E-09	1.97E-09
.60-.70	1.75E-07	1.27E-07	7.18E-08	1.43E-08	2.60E-09
.70-.80	1.91E-07	1.35E-07	8.97E-08	2.13E-08	5.88E-09
.80-.90	1.94E-07	1.41E-07	9.54E-08	3.65E-08	9.12E-09
.90-1.0	2.12E-07	1.46E-07	1.22E-07	5.50E-08	1.47E-08
1.0-1.5	2.23E-07	1.85E-07	1.40E-07	6.57E-08	2.48E-08
1.5-2.0	2.81E-07	2.46E-07	1.75E-07	9.34E-08	4.71E-08
2.0-2.5	3.41E-07	2.64E-07	2.12E-07	1.19E-07	6.95E-08
2.5-3.0	3.48E-07	3.20E-07	2.47E-07	1.53E-07	7.61E-08
3.0-3.5	3.94E-07	3.73E-07	3.30E-07	1.80E-07	1.11E-07
3.5-4.0	4.06E-07	3.90E-07	3.58E-07	2.39E-07	1.43E-07
4.0-4.5	4.87E-07	4.57E-07	3.83E-07	2.61E-07	1.20E-07
4.5-5.0	5.09E-07	5.19E-07	4.42E-07	2.65E-07	1.60E-07
5.0-6.0	5.27E-07	5.41E-07	4.62E-07	3.40E-07	1.81E-07
6.0-7.0	5.49E-07	6.37E-07	5.57E-07	3.75E-07	2.13E-07
7.0-8.0	5.73E-07	7.21E-07	6.80E-07	4.31E-07	2.86E-07
8.0-9.0	7.31E-07	8.21E-07	6.76E-07	4.83E-07	2.94E-07
9.0-10.0	8.38E-07	8.79E-07	8.20E-07	5.05E-07	3.39E-07
	Dose response function, $\frac{\text{rem}}{\text{incident proton/cm}^2}$				
.10-.15	6.45E-09	3.87E-09	1.41E-09	0.	0.
.15-.20	2.43E-07	5.18E-09	2.48E-09	2.43E-10	0.
.20-.25	3.41E-07	1.61E-08	5.83E-09	2.26E-09	9.51E-10
.25-.30	2.88E-07	2.44E-08	7.70E-09	3.07E-09	1.18E-09
.30-.35	2.71E-07	1.33E-07	1.18E-08	4.96E-09	2.12E-09
.35-.40	2.45E-07	1.88E-07	2.55E-08	6.09E-09	9.87E-10
.40-.50	1.44E-07	1.13E-07	4.39E-08	6.52E-09	1.81E-09
.50-.60	3.45E-07	2.49E-07	1.59E-07	1.93E-08	9.90E-09
.60-.70	3.70E-07	3.00E-07	1.75E-07	5.04E-08	1.31E-08
.70-.80	4.22E-07	3.40E-07	2.35E-07	7.01E-08	2.33E-08
.80-.90	4.28E-07	3.43E-07	2.60E-07	1.10E-07	3.64E-08
.90-1.0	4.89E-07	3.69E-07	3.20E-07	1.56E-07	5.34E-08
1.0-1.5	5.27E-07	4.83E-07	3.88E-07	1.90E-07	8.22E-08
1.5-2.0	5.92E-07	6.41E-07	4.86E-07	2.68E-07	1.53E-07
2.0-2.5	8.50E-07	7.16E-07	5.98E-07	3.66E-07	2.08E-07
2.5-3.0	8.84E-07	8.74E-07	7.04E-07	4.51E-07	2.42E-07
3.0-3.5	1.02E-06	1.02E-06	9.37E-07	5.45E-07	3.39E-07
3.5-4.0	1.03E-06	1.07E-06	1.00E-06	6.89E-07	4.18E-07
4.0-4.5	1.25E-06	1.25E-06	1.08E-06	7.58E-07	3.87E-07
4.5-5.0	1.29E-06	1.41E-06	1.25E-06	7.92E-07	4.77E-07
5.0-6.0	1.37E-06	1.49E-06	1.32E-06	9.88E-07	5.61E-07
6.0-7.0	1.67E-06	1.76E-06	1.60E-06	1.08E-06	6.44E-07
7.0-8.0	1.78E-06	2.02E-06	1.90E-06	1.25E-06	8.53E-07
8.0-9.0	1.97E-06	2.28E-06	1.98E-06	1.41E-06	8.84E-07
9.0-10.0	2.19E-06	2.43E-06	2.31E-06	1.52E-06	1.01E-06

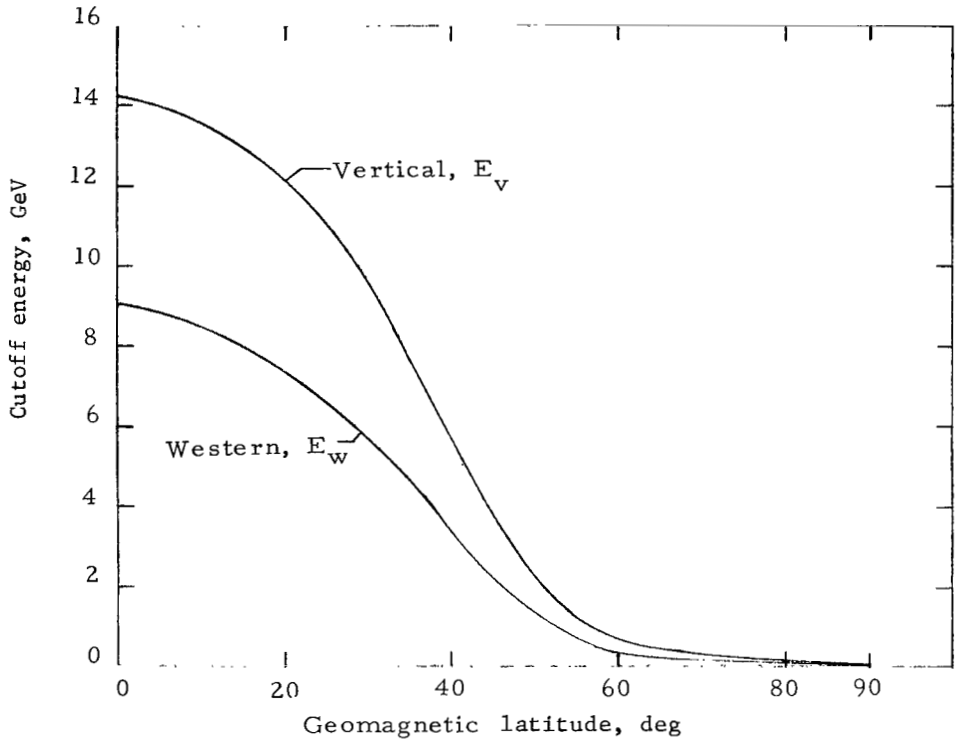

Figure 1.- Proton cutoff energy for vertical and western horizon as a function of geomagnetic latitude.

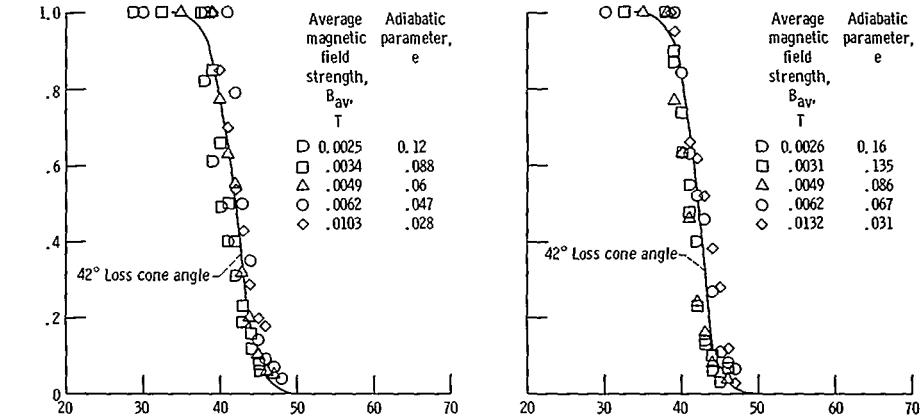

(b-1) Accelerating voltage, 400 volts; injection angle, +α.

(b-2) Accelerating voltage, 800 volts; injection angle, +α.

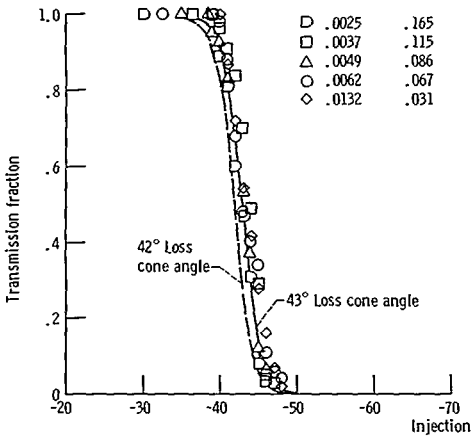

(b-3) Accelerating voltage, 800 volts; injection angle, -α.

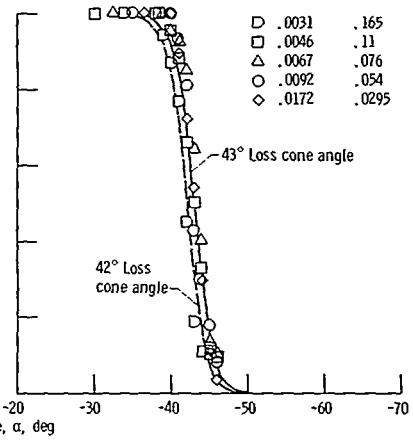

(b-4) Accelerating voltage, 1200 volts; injection angle, -α.

(b) Midplane injection radius, 4 centimeters. Curve shown is transmission fraction calculated from beam divergence measurements for loss cone angles of 42° and 43°.

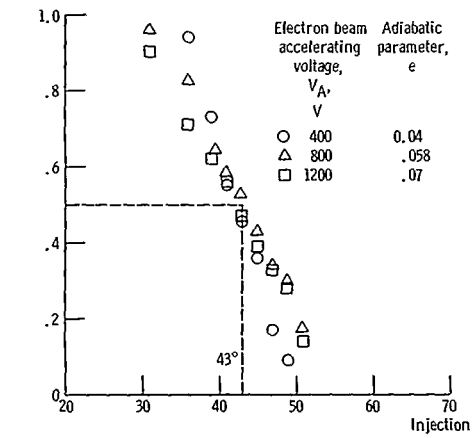

(c-1) Average magnetic field strength, 7.2×10^{-3} tesla.

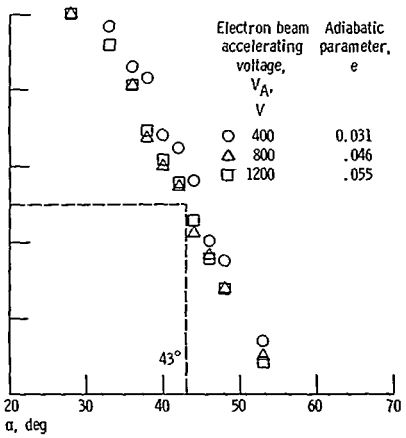

(c-2) Average magnetic field strength, 9.1×10^{-3} tesla.

(c) For an oxide cathode electron gun; injection radius, 0 at an axial position slightly behind the midplane (z = -0.5 cm).

Figure 16. - Concluded.

experimental data and the predicted results.

In figure 16(b), transmission results are presented for electrons injected at the midplane at a radial distance of 4.0 centimeters from the axis and for a range of conditions. The mirror ratio R_m (taking into account the curvature of the magnetic field lines) at a radial distance of 4.0 centimeters is 0.446. The loss cone angle associated with this mirror ratio is 42^o (eqs. (6)).

In figure 16(b-1) and (b-2) the transmission results are shown for positive injection angles. The curve calculated from the beam divergence and a loss cone angle of 42^o is also plotted on the figures for comparison. Because electrons injected off-axis at positive injection angles gyrate above the injection point, the mirror ratio for this region slightly less than 0.446 resulting in a loss cone angle slightly less than 42^o. The experimental results again agree closely with those predicted from beam divergence measurements.

In figure 16(b-3) and (b-4) the data are presented for negative injection angles, where the electrons gyrate below the injection point. In this region the mirror ratio approaches the axial mirror ratio of 0.465 which corresponds to a loss cone angle of 43^o. Calculated results are plotted for loss cone angles of 42^o and 43^o. From theoretical considerations, the data points would be expected to fall between these transmission curves. The actual data points, however, are distributed about the transmission curve for 43^o. This slight shift may be data scatter or may be the result of nonadiabatic behavior. For the range of ϵ (0.029 to 0.162) covered by the data of figure 16(b), the loss cone angle did not increase (within the 2^o spread of the data).

The transmission results presented in figure 16(c) were obtained with an electron gun positioned on axis (R = 0) but slightly behind the midplane (z = -0.5 cm). These results were used to identify any change in the transmission characteristics between a particle crossing the midplane and a particle injected at the midplane. A change in the transmission characteristics might be expected because the largest change in the magnitude of the magnetic moment occurs at the midplane. The electron gun used for these measurements was a triode gun with an oxide coated cathode. An anode aperture of 0.15 centimeter resulted in a beam divergence angle as large as $\pm 15^o$.

For the tests plotted in figure 16(c-1) and (c-2) the magnetic field was held constant while the beam accelerating voltage was varied. The beam angular distribution increased with accelerating voltage as evidenced by the changing slope of the transmission measurements. The slope of the data is constant for each accelerating voltage though, and passes through the 50 percent transmission point at a loss cone angle of 43^o. The range of ϵ for figure 16(c-1) extended from 0.04 to 0.07, and for figure 16(c-2) from 0.031 to 0.055. Within this limited range of ϵ, the results indicate that the loss cone angle did not increase as a result of injection slightly behind the midplane.

In summary, the experimental range of ϵ investigated in the course of this effort

was from 0.027 to 0.22. Results of the transmission measurements (fig. 16) indicate that the loss cone did not increase (within the 2° spread of the experimental data). For single interaction with the magnetic mirror region, particle behavior was adequately predicted by adiabatic theory. Values of ϵ considerably larger than 0.22 were not investigated with the experimental apparatus described herein because the required low magnetic field strengths (resulting in large electron gyroradius) would lead to electrons striking the magnet coil. This was found by test to occur at an $\epsilon = 0.35$. Values of ϵ below 0.02 required magnetic field strengths that distorted the distribution of the electron beam.

Previous results (ref. 13) for single interaction with a magnetic mirror using much larger magnetic fields indicated that a transition to nonadiabatic behavior would be expected for $\epsilon = 0.046$ at $R = 0$ and for $\epsilon = 0.041$ at $R = 4.0$ centimeters for a mirror ratio of 0.465. In the range of values tested and reported herein, which extends both above and below the indicated adiabatic transition value of ϵ, no evidence of an increase in the loss cone was found.

CONCLUDING REMARKS

Nonrelativistic single particle behavior was experimentally investigated in an axisymmetric mirror magnetic field. Measurements were made on an electron beam for a single interaction with the mirror region. Within the 2° spread of data of this investigation, the loss cone angle for a single interaction of electrons with a mirror field was not observed to increase (i.e., to become noticably nonadiabatic) for a range of the adiabatic parameter ϵ from 0.027 to 0.22.

Lewis Research Center,
National Aeronautics and Space Administration,
Cleveland, Ohio, June 25, 1970,
120-26.

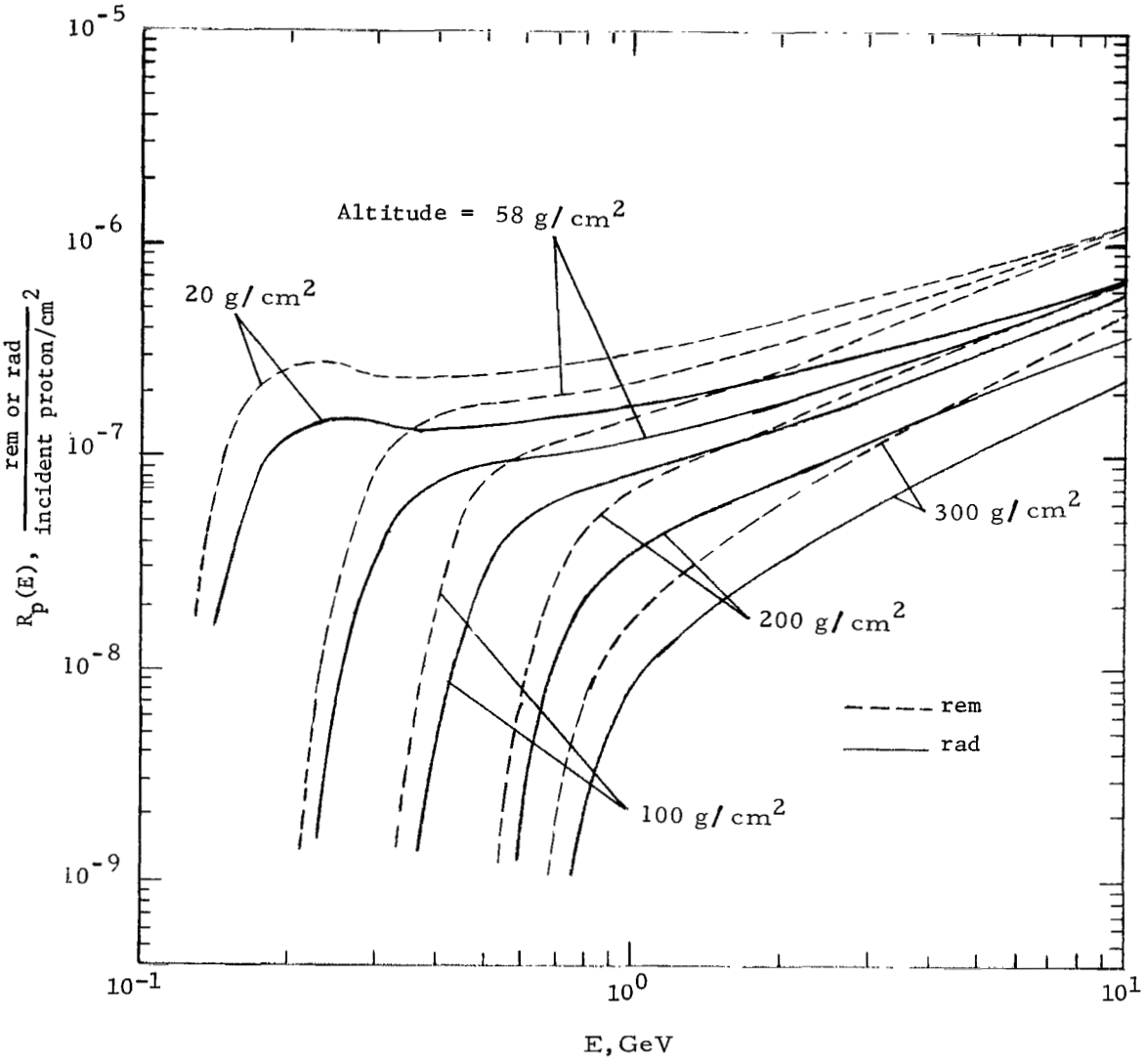

Figure 5.- Proton extremity dose response functions due to incident protons at various altitudes. (Note the Bragg peak at 20 g/cm^2.)

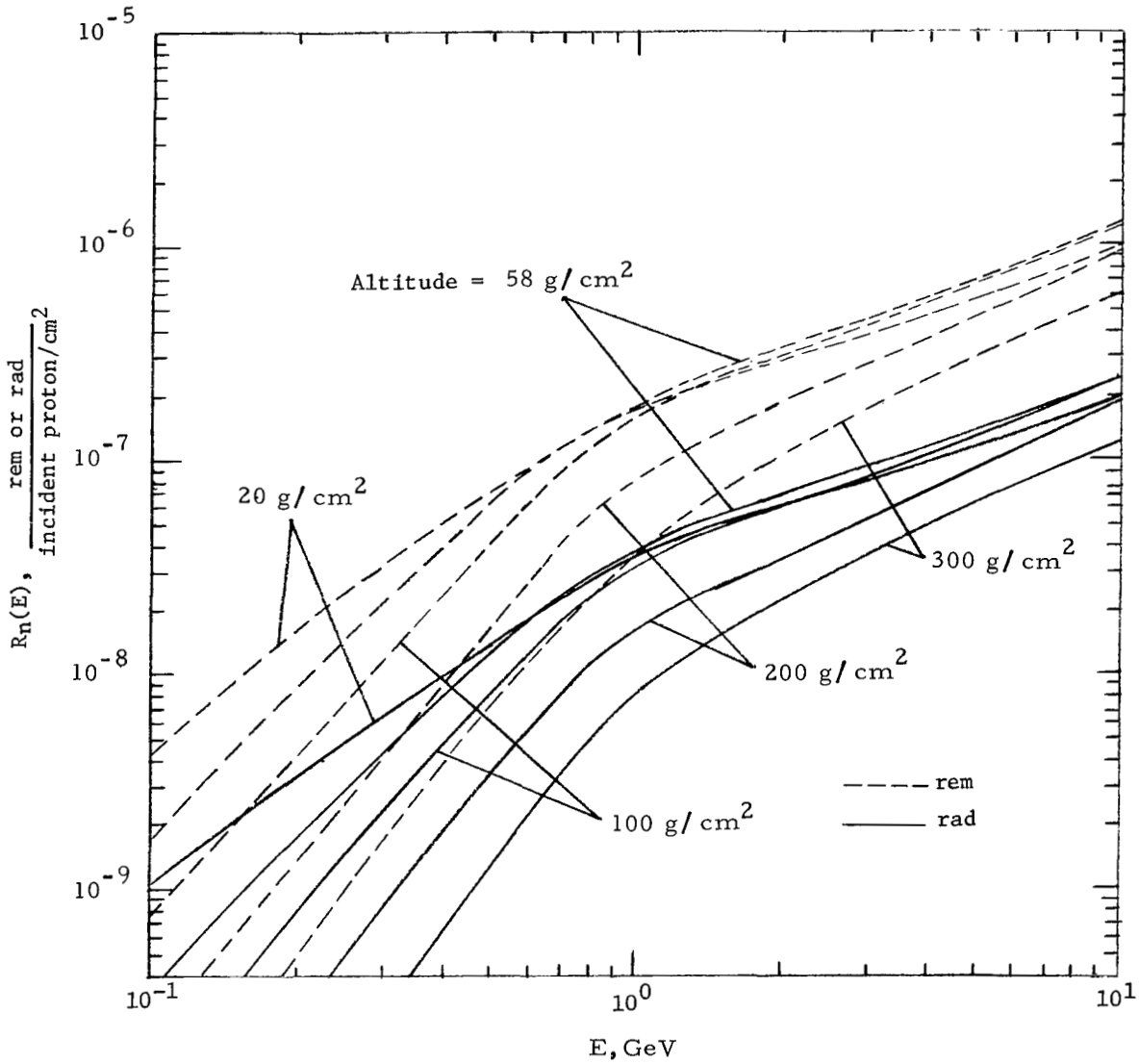

Figure 6.- Neutron extremity dose response functions due to incident protons at various altitudes.

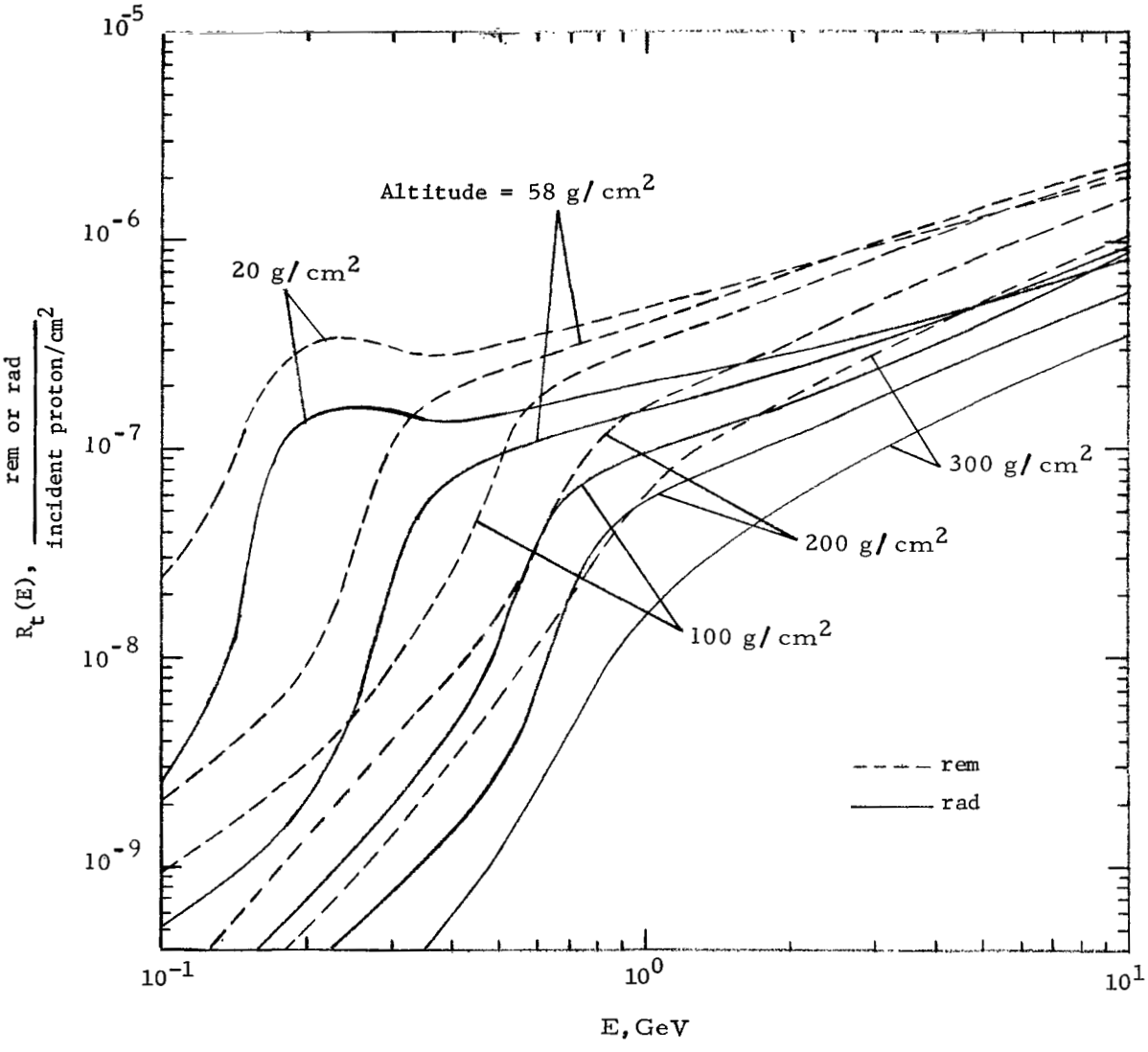

Figure 7.- Total extremity dose response functions due to incident protons at various altitudes. (Note the Bragg peak at 20 g/cm^2.)

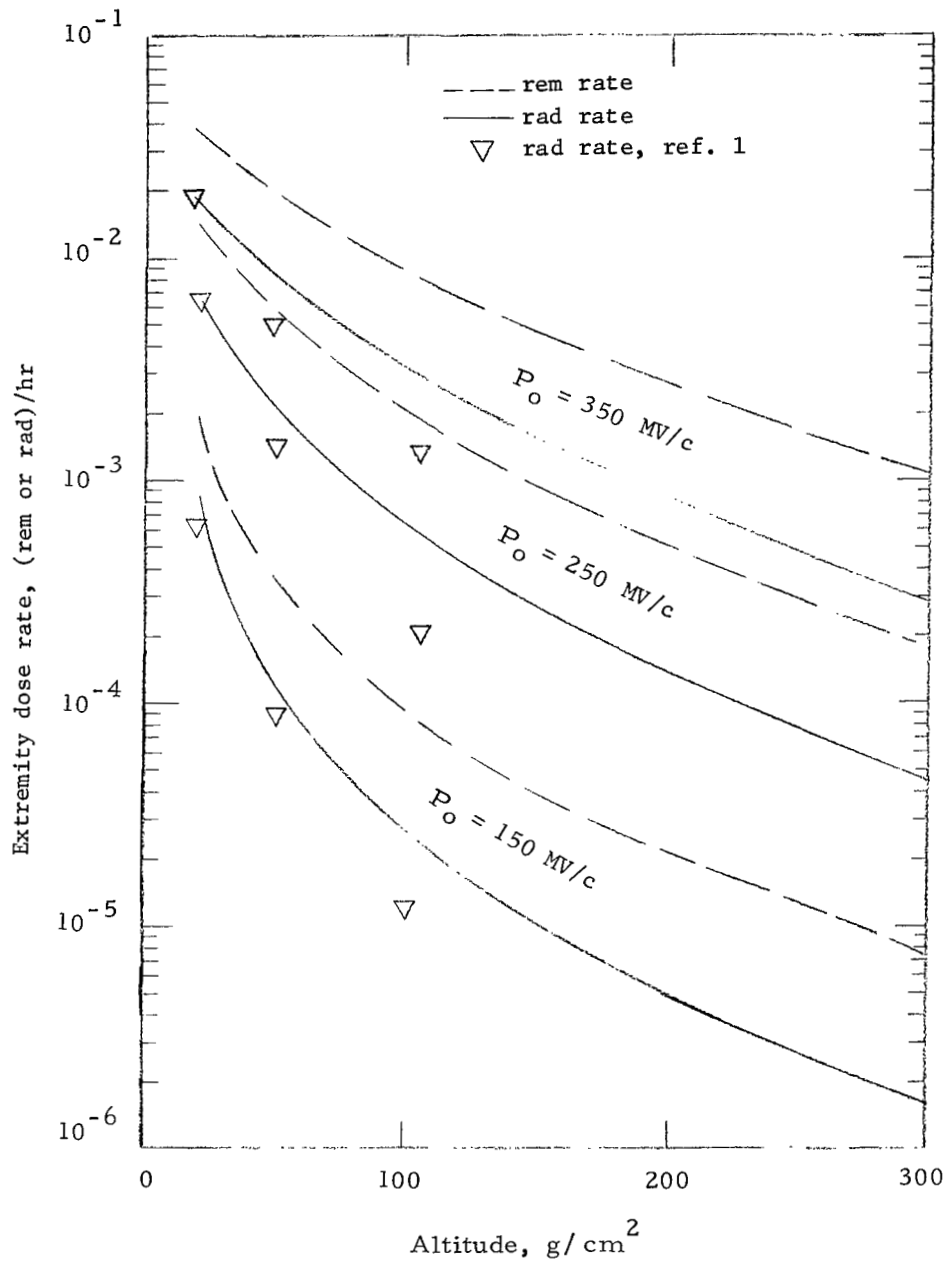

Figure 8.- Dose rates in extremities as a function of altitude for three P_o spectra.

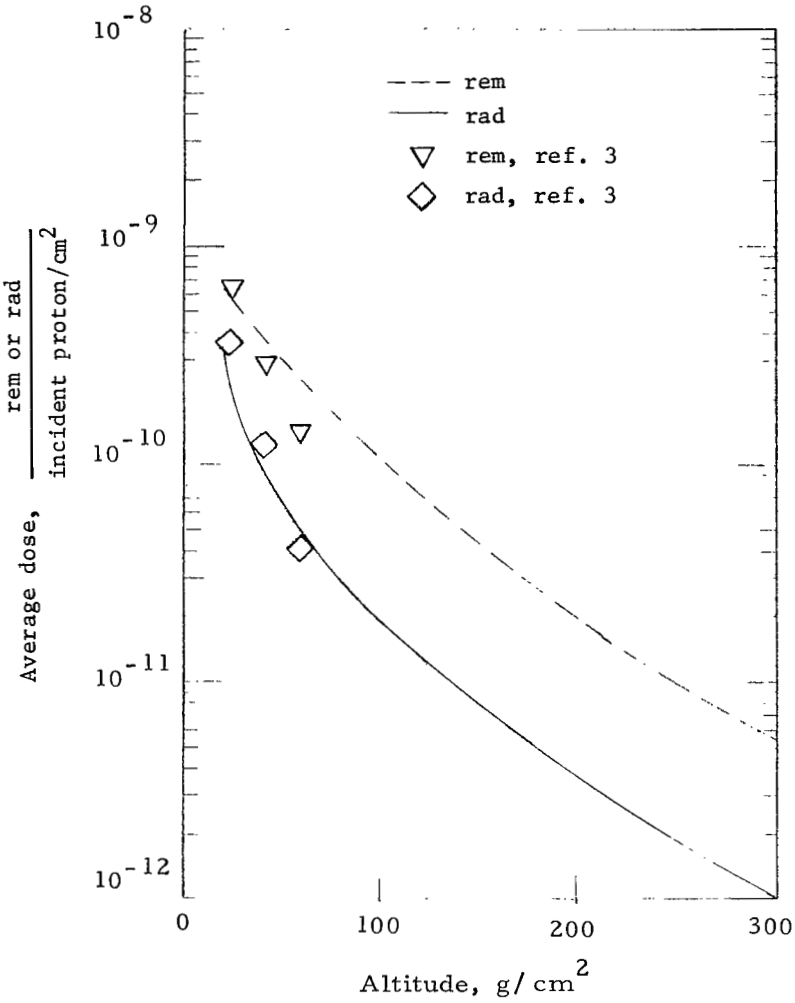

Figure 9.- Dose averaged over the whole body per unit flux as a function of altitude. P_o = 100 MV/c.

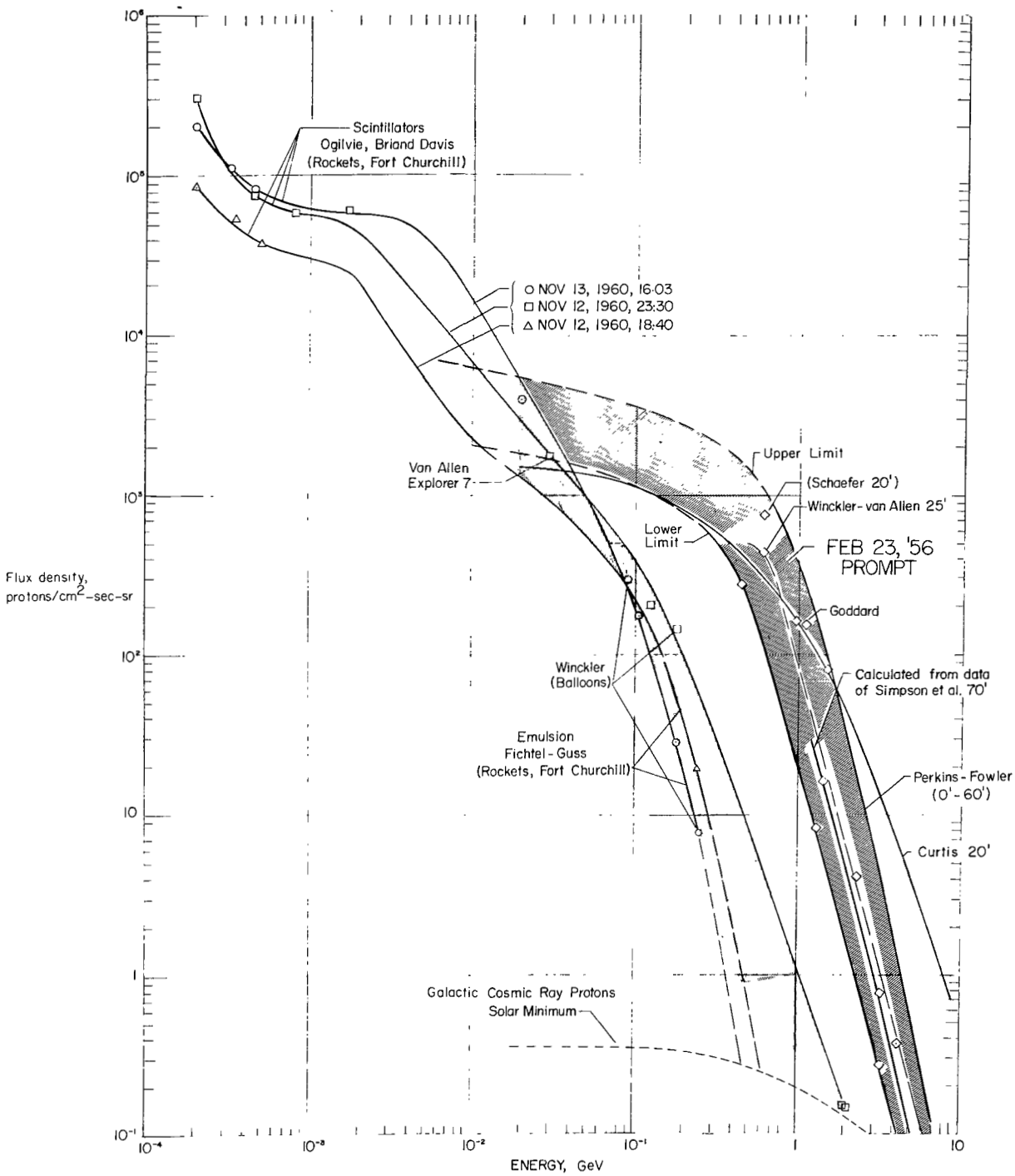

Figure 10.- Integral-energy flux density for extreme solar events of solar cycle 19.

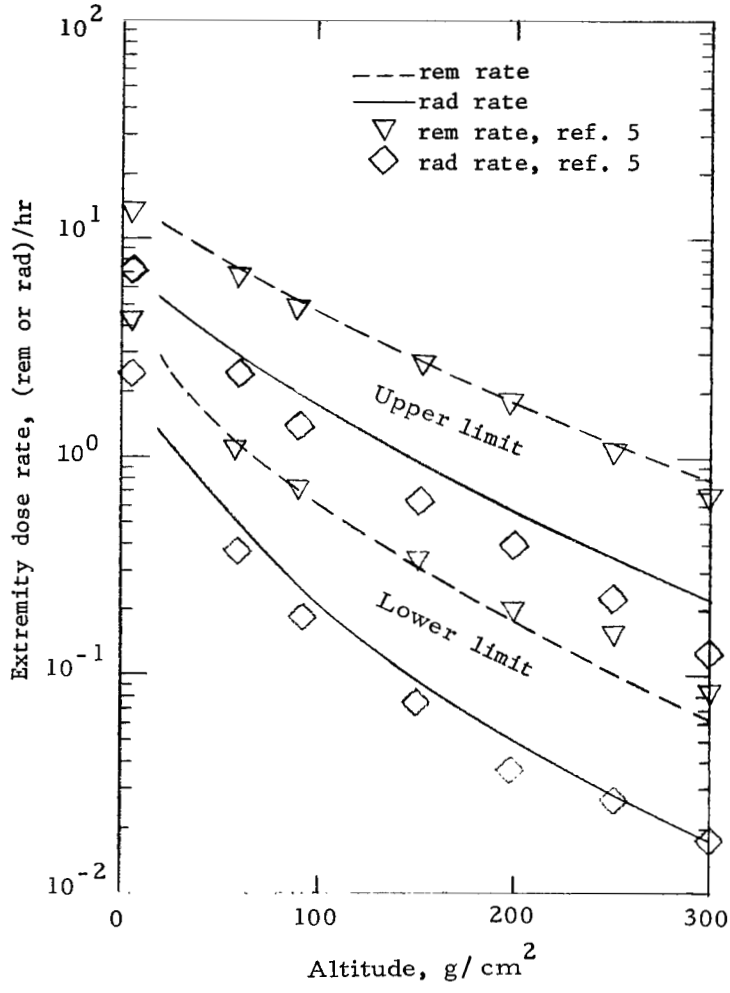

Figure 11.- Upper and lower limits of dose rate in extremities for the prompt spectrum of the February 1956 solar event.

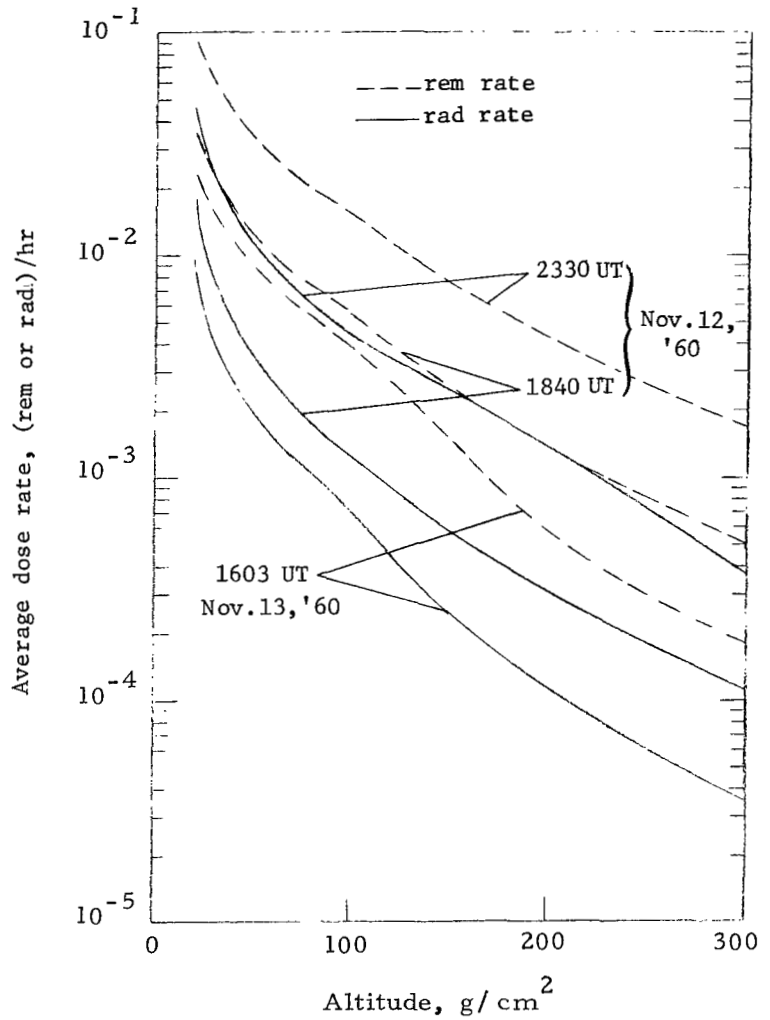

Figure 12.- Dose rate averaged over the whole body for the solar event of November 12, 1960.

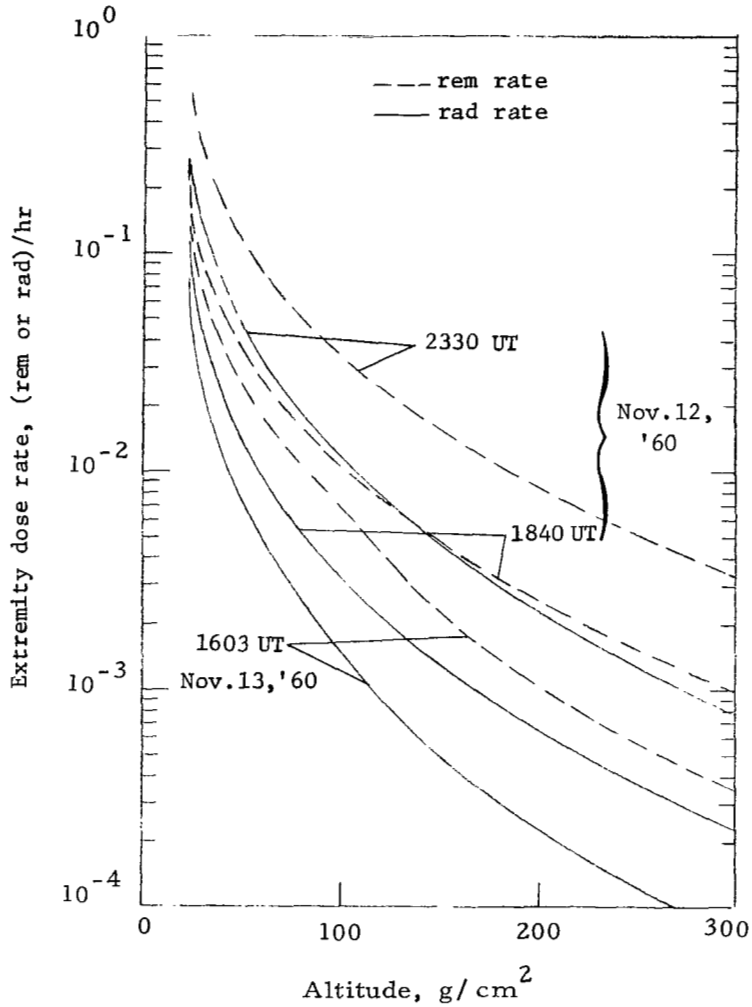

Figure 13.- Dose rate in extremities for the solar event of November 12, 1960.

"The aeronautical and space activities of the United States shall be conducted so as to contribute . . . to the expansion of human knowledge of phenomena in the atmosphere and space. The Administration shall provide for the widest practicable and appropriate dissemination of information concerning its activities and the results thereof."

—NATIONAL AERONAUTICS AND SPACE ACT OF 1958

NASA SCIENTIFIC AND TECHNICAL PUBLICATIONS

TECHNICAL REPORTS: Scientific and technical information considered important, complete, and a lasting contribution to existing knowledge.

TECHNICAL NOTES: Information less broad in scope but nevertheless of importance as a contribution to existing knowledge.

TECHNICAL MEMORANDUMS: Information receiving limited distribution because of preliminary data, security classification, or other reasons.

CONTRACTOR REPORTS: Scientific and technical information generated under a NASA contract or grant and considered an important contribution to existing knowledge.

TECHNICAL TRANSLATIONS: Information published in a foreign language considered to merit NASA distribution in English.

SPECIAL PUBLICATIONS: Information derived from or of value to NASA activities. Publications include conference proceedings, monographs, data compilations, handbooks, sourcebooks, and special bibliographies.

TECHNOLOGY UTILIZATION PUBLICATIONS: Information on technology used by NASA that may be of particular interest in commercial and other non-aerospace applications. Publications include Tech Briefs, Technology Utilization Reports and Notes, and Technology Surveys.

Details on the availability of these publications may be obtained from:

SCIENTIFIC AND TECHNICAL INFORMATION DIVISION

NATIONAL AERONAUTICS AND SPACE ADMINISTRATION

Washington, D.C. 20546